Optical Activity of Achiral Ligand SCH_3 Adsorbed on Achiral Ag_{55} Clusters: Relationship between Adsorption Site and Circular Dichroism

Francisco Hidalgo and Cecilia Noguez*

Instituto de Física, Universidad Nacional Autónoma de México, Apartado Postal 20-364, México D.F. 01000, México

ABSTRACT The electronic circular dichroism (CD) spectra of a methyl-thiol adsorbed at different sites on an icosahedral silver nanoparticle is studied by using time-perturbed density functional theory. Despite that separately molecule and nanoparticle are achiral and consequently optically inactive, the Ag_{55}—SCH_3 compound emerges with a new symmetry, which may be chiral or not depending on the adsorption site and orientation of the molecule. It is found that chirality is favored when the thiol is adsorbed between two atoms of different coordination number. Chiral compounds have characteristic CD spectra in the UV—visible region, where Ag_{55} shows optical absorption but SCH_3 does not; revealing that highly degenerated molecular-like electronic states of Ag_{55} are modified by the presence of the molecule inducing optical activity. It is concluded that CD line-shapes and magnitude strongly depend on the site where the adsorption takes place, while its intensity is modulated by the molecule orientation.

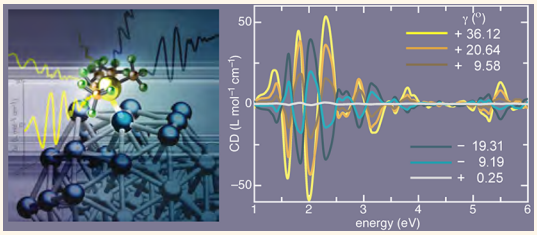

KEYWORDS: ligand-protected metal nanoparticles · chirality · circular dichroism · thiol adsorption · silver nanoparticle · dissymmetric field

Metal nanoparticles (NPs) exhibit amazing physical and chemical properties, such as optical,[1] electronic,[2] and catalytic,[3] which have opened new research fields with interesting applications in biophysics, medicine, pharmacology, and materials science.[4] These properties strongly depend on size, shape, and atomic species composing NPs; parameters that are crucial to design specific nanoscale devices with uniform properties.[5−7] Among these properties, optical activity is relevant for new chiral science and technology developments,[8] for enantioselectivity processes,[9] structural DNA self-assembly nanotechnology,[10] and other interesting applications. Chirality is a geometrical property that consists in the impossibility of making coincide the original object with its ideally realized image in a plane mirror. This means that both objects are nonsuperposable and they are called enantiomers.[11] Furthermore, chirality is a property present at the nanoscale, for instance in fullerenes, nanotubes, and metal NPs;[12] and circular dichroism (CD) has risen as an important tool to study optical activity in these systems.[13−17]

Metal NPs, like gold and silver, are usually unsteady and need to be stabilized by adding certain kind of ligands on their surface; frequently adsorbing thiol molecules.[18] This passivation can lead to atomically precise NPs,[19] which are of fundamental importance to understand the evolution of electronic and optical properties as a function of size and morphology.[20] In these ligand-protected metal NPs a whole new range of optical properties have been observed, in particular, optical activity has been measured when chiral and achiral ligands are employed. Since the first observation of optical activity[21] and its later confirmation using different NPs and ligands,[22−26] different groups have investigated its origin.[27−38] For instance, there have been proposed atomic chiral configurations for bare and/or ligand-protected Au_{38}, Au_{28}, and Au_{34}^- clusters that show intense optical activity due to the strong distortion of the metallic part.[27,28] However, the higher symmetric cluster $[Au_{25}(SR)_{18}]^-$ protected with different ligands (R),[31,32] also shows a significant optical activity.[33] In this case, a theoretical

* Address correspondence to cecilia@fisica.unam.mx.

Received for review October 4, 2012 and accepted December 20, 2012.

Published online December 20, 2012
10.1021/nn3046083

© 2012 American Chemical Society

study concluded that CD signals not only come from the structural distortion of the metallic core, but also from a dissymmetric field created by the ligands, which not only induces chirality, but also enhances the CD signal coming from the slight structural distortion of the metallic core, where both mechanisms are acting concurrently.[34] It was also found that optical activity is mainly due to the overall chiral geometry of the organo-metallic compound, and quite independent of whether the ligands are chiral or not.[20,34] This theoretical prediction has been recently confirmed by the enantioseparation and measurement of CD spectra of Au_{38} clusters protected by achiral ligands.[36]

Similarly, morphology has been found to be also relevant in the optical activity and enhancement of CD signals when silver NPs are used instead of gold.[38−42] Chiral biomolecules conjugated with large silver NPs (~23 nm in size) also show characteristic CD signals.[39] For instance, thiol group-containing biomolecules, such as cysteine, glutathione, and penicillamine with silver NPs produce CD signals in the region of 240−400 nm (*ca.* 3−5 eV). Here, cysteine is somehow interacting with Ag colloids to cause new conformational arrangements, generating characteristic CD signals in the optical absorption region of silver. Also, a critical concentration of cysteine molecules was found, where the characteristic CD signal is observed, but it decreases upon the increment from a critical concentration. The L-cysteine mixed with large silver NPs form a chiral complex; this not only exhibits a different CD spectrum with respect to its components, but also a time-dependent CD intensity.[40] Furthermore, silver NPs with L-GS-bimane ligands not only show an enhanced CD signal, but also an enhanced optical absorption,[41] where the enhancement of both signals strongly depend on NP size. The possibility to obtain enhanced CD spectra, in analogy to surface-enhanced Raman scattering (SERS) phenomenon,[42] has attracted attention, because CD has a moderate sensitivity, which hampers the analysis of chiral molecules at low concentrations and/or low enantiomeric excess. However, it has been suggested that chiral NP complexes could offer the possibility to create strong optical activity in the visible region.[38] The study of optical activity in silver compounds not only might result relevant for new chiral science and technology, but also opens the possibility of new spectroscopic chiroptical tools.

Despite the theoretical and experimental efforts done up to now, all these results in gold and silver ligand-protected NPs show a complicated relationship between the resulting optical activity of the compounds and the nature of their components, that is, NPs and ligands. In this paper, we are interested in explaining the origin of this chiroptical signal and its possible enhancement, as well as its relationship with the metal NP, the location of the ligands, and their orientations. As a starting point, we present a study of

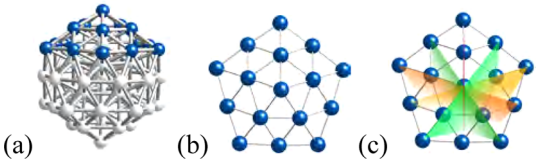

Figure 1. (a) The Ag_{55} NP. (b) The pentagonal top arrangement and (c) its five σ planes, which are aligned over the five edges.

Figure 2. (a) SCH_4 shows one σ plane and (b) SCH_3 shows three σ planes. S in yellow, C in brown, and H in green.

CD spectra of a single achiral molecule adsorbed at different sites and with different orientations on an achiral cluster, using time-perturbed density functional theory. Our goal is to find the main mechanisms that give rise to optical activity in ligand-protected NPs, and how CD spectra line-shape and intensity are modulated by geometrical end electronic interactions.

RESULTS AND DISCUSSION

We consider a NP formed by 55 silver atoms with icosahedral symmetry, as seen in Figure 1a where the pentagonal top arrangement is shown with blue atoms. Icosahedra have 20 faces (equilateral triangles), 12 vertices, and 30 edges. All faces, vertices, and edges are symmetrically equivalent, respectively.[43] The Ag_{55} icosahedral NP comprises 13 atoms in the core-nucleus and 42 atoms on the surface, where each face contains 6 atoms. The 13 atoms in the core have 12 first nearest-neighbors, such that their coordination number is 12. In the outside shell, vertex atom are always shared by five faces, as shown in the top view of the pentagonal top arrangement in Figure 1(b), and their coordination number is 6, while edge atoms are shared by only two faces and have a coordination number 8. Figure 1c shows five σ (mirror) planes on the pentagonal top arrangement of the icosahedron.

We assume that a SCH_4 molecule is adsorbed at the surface of Ag_{55}. This molecule has one σ plane, which is formed by the H−S−C−H atoms shown in Figure 2a. The thiol group on the metallic surface is adsorbed through the sulfur atom. Therefore, upon adsorption, one of the H atoms of SCH_4 is removed, and now the adsorbed SCH_3 molecule exhibits three symmetry planes each one formed by the S−C bond and each one of the three H atoms of the methyl, as seen in Figure 2b. By the above description, both the Ag_{55} cluster and the SCH_4 and SCH_3 molecules are achiral, so separately they do not show any optical activity.

The Ag_{55}−SCH_3 compound is built by adsorbing the thiol group, such that S is binding to the metallic NP

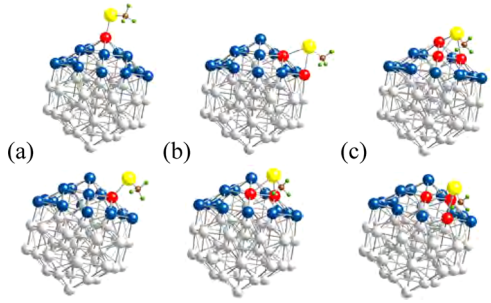

Figure 3. (a) Top (bottom) model corresponds to the top−vertex (top−edge) configuration. (b) Top (bottom) model corresponds to the bridge−edge (bridge−face) configuration. (c) Top (bottom) model corresponds to the hollow−vertex (hollow−face) configuration. Ag atoms involved in the adsorption are in red.

with Ag−S bond lengths of about 2.5 Å, according to previous DFT calculations of small silver clusters with thiol molecules.[44] SCH_3 is bonded using as a guide an imaginary line that joints the S atom, the adsorption site, and the mass center of the NP. Because of high symmetry of Ag_{55}, there are three different types of adsorption sites, and each one has two different possibilities. In Figure 3a the top−atom case is shown, where the adsorption site corresponds to one Ag atom in the NP, with two different possibilities of top−atoms: when the atom is on a vertex (top−vertex case) and when the atom is on an edge (top−edge case); both cases are shown in the top and bottom of Figure 3a, respectively. The first case has 12 equivalent sites, while the second one has 30. We also have the bridge case that corresponds to an adsorption site located between two nearest-neighbor Ag atoms, also with two different possibilities: when both Ag atoms belong to the same edge (bridge−edge case) and when both Ag atoms are on different edges (bridge−face case), as shown in the top and bottom of Figure 3b, respectively. Both configurations have 60 equivalent sites. Finally, we have the hollow case that corresponds to an adsorption site located in the middle of three nearest-neighbor Ag atoms, again with two different possibilities: when one Ag atom forming the hollow is on a vertex (hollow−vertex case), having 3 equivalent places for each face, so there are 60 equivalent sites; and when neither Ag atom is a vertex (hollow−face case) with one possibility for each face, with a total of 20 equivalent sites. Both hollow−vertex and hollow−face cases are shown in the top and bottom of Figure 3c, respectively.

For each one of the six possible cases described above, the SCH_3 molecule can have different orientations around the adsorption axis; however, not all these configuration are stable, as we discuss below. Therefore, we have performed molecular dynamic simulations over a large number of initial configurations to obtain the lower-energy Ag_{55}−SCH_3 compounds, which is fundamental to understand chirality and optical activity. We have found that the lowest-energy configuration is for the bridge−face case, while the top−vertex case is the configuration with largest energy, showing a difference of ΔE = 0.964 eV between them. The large energy difference between top and bridge cases can be associated to the distortion of the icosahedral symmetry suffered by Ag atoms when the molecule is adsorbed in top configurations, as well as the different coordination number of vertex (8) and edge (6) atoms. While the largest atomic position deviation from the icosahedral geometry in the top−vertex configuration is about 2.2%, for the bridge configurations it is less than 0.8%. On the other hand, the difference in the coordination number of top and vertex atoms can substantially change the electronic conditions around the adsorption site. The bridge−face and both hollow cases, vertex and face, are very close in energy with ΔE = 0.002 eV. This is because hollow configurations upon relaxation experiment a drastic change in the position of the molecule, ending mostly in bridge−face. Since these configurations are very similar to those found for the bridge cases, the optical activity and absorption spectra are almost identical to those for the bridge cases. However, subtle effects can be seen, as we will discuss later.

TABLE 1. Energy Differences (ΔE) between the Lowest-Energy Isomer and the Rest. The Maximum Energy Variation (δE_{max}) as a Function of Molecule Orientation for Each Case Is Also Shown

case	ΔE (eV)	δE_{max} (eV)
top−vertex	0.964	0.009
top−edge	0.698	0.042
bridge−edge	0.130	0.570
bridge−face	0.000	0.112
hollow−vertex	0.002	0.172
hollow−face	0.001	0.148

In Table 1, the energy differences between isomers and the lowest-energy configuration, the bridge−face case, are shown. The maximum energy variations δE_{max} due to different molecule orientations is also included. Both top cases show very small variations δE_{max}, as compared with the rest of the cases. This means that the CH_3 orientation does not play an important role in the top final configuration, but it does in the optical activity as we will discuss latter. Finally, δE_{max} is larger for bridge and hollow cases, which means that the stability of these configurations strongly depends on the molecule orientation. As a consequence, we find that some configurations are not stable. In this paper, we are interested in the optical activity in terms of the morphology of Ag_{55}−SCH_3. A detailed discussion of the atomic arrangements of the most stable configurations will be discussed elsewhere.

We start discussing the optical absorption and optical activity of the silver cluster and molecule as

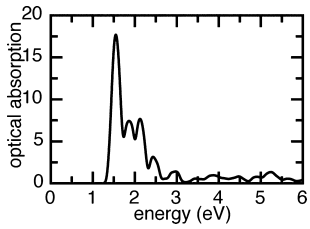

Figure 4. Optical absorption of the Ag_{55} cluster after relaxation.

separate units. In the energy region of interest, that is, from 0.5 to 6 eV, we found that the molecule does not show any significative optical absorption, and the optical activity is null. The Ag_{55} cluster shows optical absorption peaks that are characteristic of electronic transitions associated to degenerate molecular-like states. This degeneracy originates from highly symmetric atomic arrangements. In Figure 4 we show the optical absorption spectrum of bare Ag_{55} after relaxation with well-defined peaks due to electronic transitions from occupied to empty states. The highly symmetric cluster does not show optical activity. As follows, we discuss the optical activity and optical absorption of the different $Ag_{55}-SCH_3$ isomers described in the previous section.

First, we present the geometrical and optical properties of both top configurations, which allow us to understand the role that symmetry plays in determining optical activity. In the top−vertex case the 5-fold symmetry planes of Ag_{55} intersect each other at the vertex atom where the adsorption takes place, such that rotations by $\pi/5$ are present, see Figure 1c. On the other hand, for the top−edge case the adsorption site is not at the center of the pentagon motif or vertex, but at the middle of an edge. Then, there are only two symmetry planes, which are perpendicular to each other, giving rotations of $\pi/2$. Another important ingredient in describing symmetry is the orientation of the molecule with respect to the symmetry planes. Therefore, we define γ as the smallest angle between any symmetry plane of SCH_3 and anyone of Ag_{55}, where both planes are mutually intersected. In this way, a configuration with $\gamma = 0$ is found when one symmetry plane of Ag_{55} matches one of the molecule, such that at least one symmetry plane is preserved and the configuration is achiral, as shown in Figure 5b for the top−vertex and top−edge cases. On the other hand, Figure 5a and Figure 5c in the top row show low-energy top−vertex isomers with orientations, such that none of the symmetry plane of SCH_3 coincide with any of Ag_{55}. In the bottom row similar configurations are shown for the top−edge case. The off-alignment ($\gamma \neq 0$) breaks the total symmetry allowing isomers be chiral and so, optically active. For these chiral configurations, we assign negative values of γ when the molecule points to the counterclockwise direction with respect to the achiral configuration,

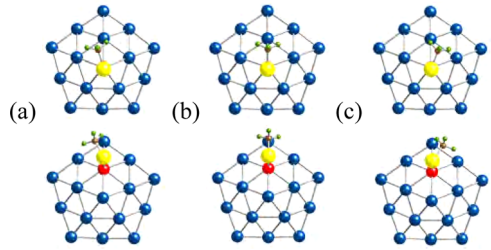

Figure 5. Low-energy configurations for top cases. Top row shows top−vertex isomers and bottom row shows top−edge isomers. While structures a and c are enantiomers, respectively, structures b are achiral configurations. To distinguish the atoms involved in adsorption, they are in red.

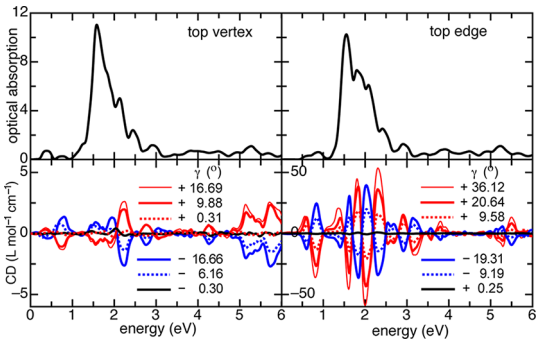

Figure 6. Optical absorption and CD spectra of the $Ag_{55}-SCH_3$ compounds for top−vertex and top−edge cases.

shown in Figure 5a, while Figure 5c corresponds to positive ones (clockwise direction).

The optical absorption spectra for both top cases, shown in the top of Figure 6, exhibit smaller optical gaps than that found for the bare cluster (see Figure 4). Here, optical absorption is found below 1 eV because the cluster symmetry is broken, the degeneracy is partly lost, and then, the molecular-like electronic states are spread out. Therefore, the intensity of the main peak at about 1.55 eV is decreased by nearly 40%, and the well-defined peak structure is lost in part, mainly between 1.5 and 2.5 eV. For each case it is found that optical absorption is exactly the same independently of the molecule orientation, that is, it is not possible to distinguish the configurational differences between chiral and achiral systems. Therefore, the molecule orientation cannot be deduced from the absorption spectra. However, we will show that this local property can be inferred from CD spectra.[45]

In the bottom row of Figure 6, CD spectra of top−vertex and top−edge isomers with six different γ angles are shown. From both CD spectra, we observe the following: (a) CD is present at the same energy range than optical absorption occurs and CD peaks are at energies where the optical absorption of bare Ag_{55} was modified upon molecule adsorption. (b) Isomers with smallest γ show CD spectra that are almost null, like that which corresponds to achiral configurations.

Furthermore, CD of isomers with negative γ are the same but of opposite sign to those with equivalent positive γ. We conclude that isomers with the same γ value but opposite sign behave like enantiomers, where the molecule symmetry plane is rotated equally but in opposite direction from a symmetry plane of Ag_{55}. (c) An interesting feature of these results is that the line-shape of the spectra is similar for all molecule orientations. However, the intensity of the spectra varies as a function of γ, where the maximum intensity is found for the largest possible value. For instance, in the top−vertex case the maximum intensity is found when γ is between two symmetry planes, that is, when γ takes values close to $\pm\pi/10$. For the top−edge case, the maximum would be observed when γ is approaching the value between two symmetry planes ($\pm\pi/4$). However, this situation never happens because the system becomes very unstable for values larger than *ca.* $\pm 36°(\pi/5)$.

The CD signal from top edge cases shows an intensity which is about 20 times larger than that exhibited by top−vertex. Also, CD line-shapes are quite different for each case, although the maximum intensity is reached at around 2 eV in both configurations. The differences in both chiroptical signals could be attributed to geometrical and electronic factors. For instance, to the proximity of CH_3 to the metallic surface in the top−edge case, or to the fact that top−edge has lower symmetry than top−vertex. Also notice that the electronic environment in each is different: edge atoms exhibit larger coordination number (8) than vertex atoms (6) that lead to more or less degenerated electronic states, which might be broken differently upon molecule adsorption due to the strong binding in the Ag−S bond, as we will discuss latter.

Let us analyze the bridge cases which are those found to be of lowest energy. Both bridge cases have only one symmetry plane in the adsorption site, so that only symmetry rotations by π are present. For the bridge−edge, achiral configurations occur when the molecule is aligned along the bridge formed by the two Ag atoms involved in the adsorption, with two possible orientations: CH_3 pointing to the vertex atom or, in opposite direction, to an edge atom. This latter configuration is shown in top of Figure 7b. However, these achiral configurations have larger energy, while low-energy configurations are obtained when the molecule is off-aligned to the bridge (Figure 7a,c); that is, bridge−edge chiral configurations are more stable. The molecule adsorption occurs between two Ag atoms belonging to the same edge where one is a vertex atom and the other is an edge atom, with coordination numbers of (6) and (8), respectively. The difference in coordination number of both atoms can favor chiral configurations.[9] The two chiral bridge −edge configurations before and after relaxation in the top and bottom of Figure 7a,c are enantiomers.

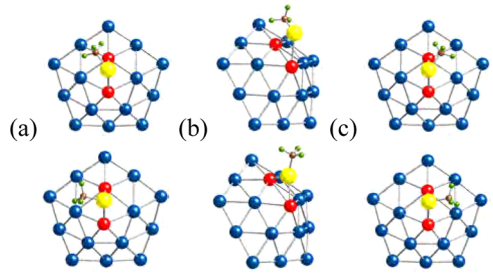

Figure 7. Bridge−edge configurations. Top (bottom) row corresponds to initial (relaxed) configurations, structures a and c are enantiomers, while structures b correspond to an achiral case that observes high energy.

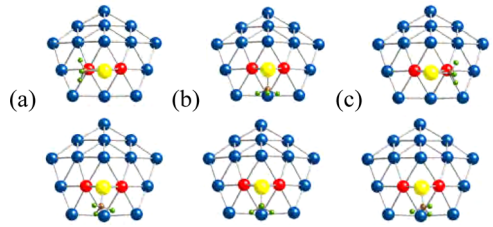

Figure 8. Bridge-face configurations. Top (bottom) row corresponds to initial (final) configurations. Structures a and c are enantiomers, while structures b correspond to an achiral case.

Comparing configurations before and after relaxation, it is observed that not only CH_3 rotates around the adsorption site, but also a rotation around the S−C axis is found. This means that the orientation of hydrogens is changed, and then, the orientation of the molecule's symmetry planes. Although important changes are achieved, at the end of the relaxation process both isomers are still enantiomers differing in energy each other by only 0.004 eV.

For the bridge−face, achiral cases occur when the molecule is aligned perpendicular to the bridge, having two possibilities. The first is when SCH_3 is pointing to a vertex atom, which is not stable because it has an energy of $\delta E = 0.112$ eV above the most stable isomer. The second achiral configuration is when the molecule points to an edge atom, as depicted in Figure 8b, and which is only $\delta E = 0.007$ eV with respect to the lowest-energy configurations shown at the bottom of Figure 8a,c, which are chiral isomers. These chiral configurations are obtained from a drastic change upon relaxation of the initial configurations shown at the top of Figure 8a,c, respectively. Here, initially SCH_3 is parallel to the bridge, but after relaxation the molecule rotates almost 90° around the adsorption site, and at the same time hydrogens also rotate around the S−C axis, resulting that SCH_3 is slightly out of the Ag_{55} symmetry plane. After this significant change both isomers are still enantiomers and they differ in energy by only 0.002 eV.

The top row of Figure 9 shows the optical absorption spectra for both bridge cases with optical gaps of

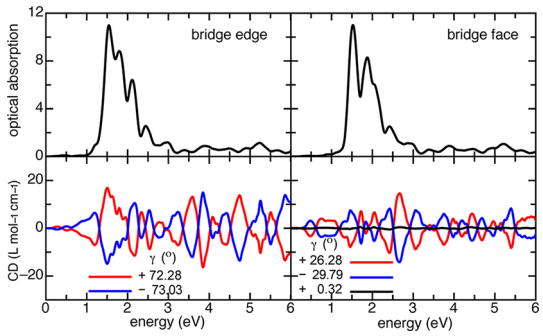

Figure 9. Optical absorption and CD spectra of the Ag_{55}−SCH_3 compound for bridge−face and bridge−edge cases.

about 1 eV. Similar to the top cases, both absorption spectra are quite independent of the molecule orientation. Again, the symmetry of the cluster is broken by the presence of the molecule, such that electronic states are spread out, the intensity of the main peak decreases, and the well-defined peak structure is partly lost. The bottom row of Figure 9 exhibits CD spectra of low-energy isomers for both bridge cases. Here, red and blue spectra correspond to the relaxed chiral enantiomers, which have positive and negative similar γ angles (see isomers a and c in both Figure 7 and Figure 8). It is confirmed that CD spectra only differ by a sign, as γ also does. The black line in the bridge−face CD spectra belongs to the achiral configuration that shows a very small γ angle. We recall that due to the strong dependence of the isomer stability with the molecule orientation for both bridge cases, it is not possible to obtain many different γ values as we did for both top cases.

Here, CD intensities are about half of that of top−edge, but they are about ten times more intense than the top−vertex case. Considering the results discussed for top cases and the fact that bridge configurations exhibit only one symmetry plane, we would expect to obtain the maximum intensity when $\gamma = \pm\pi/2$. While bridge−edge isomers can be closed to this value, chiral bridge−face isomers reach less than a third of $\pi/2$. Notice that in the bridge−face case, the molecule adsorption occurs between two edge atoms, such that they have the same coordination number (8). This fact contributes to the stability of the isomers, but γ is restricted to small values. Despite this difference, CD intensities are not so different in contrast to top cases. Also, line-shapes of both bridge cases exhibit positive−negative structures in a larger energy region. Moreover, CD spectra show a quite even intensity along all the energies, and there is not a dominant peak or peaks. Furthermore, the line-shapes of both bridge CD spectra are quite different. Below, we will discuss how these differences are related to how the electronic degeneration is broken after molecule adsorption.

We have seen that the lowest-energy configuration of $Ag_{55}SCH_3$ is the bridge−face case, when the

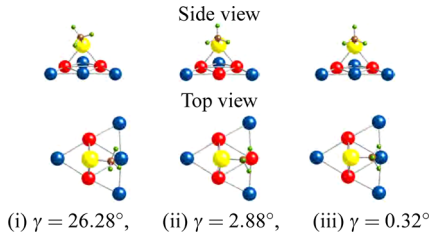

Figure 10. Lower-energy bridge−face isomers obtained from different bridge face and hollow face initial configurations.

TABLE 2. Structural Parameters of Bridge Face Configurations after Relaxation

isomer	Ag(1)−S−C (deg)	Ag(2)−S−C (deg)	γ (deg)	ΔE (eV)
i	112.39	106.75	26.28	0.000
ii	111.00	108.43	2.88	0.006
iii	109.75	109.46	0.32	0.007

molecule is almost aligned perpendicular to the bridge, as shown in Figure 8. Similar isomers with almost equal energy can be found using different initial configurations, for instance, in the bridge face when initially the molecule is pointing along the bridge to the left-or to the right-hand side, or when the initial configuration is a hollow vertex. Although all these isomers are quite similar, we observe that the hydrogens forming the methyl suffer different rotations after relaxation depending on the initial configuration. This fact can explain the small energy differences up to 0.002 eV found between isomers. Figure 10 shows side and top views of the molecule and the Ag_{55} face involved in the adsorption for the three different bridge−face configurations described above. The first case, Figure 10i corresponds to the chiral bridge face of lowest energy and described in Figure 8a, while Figure 10ii was obtained by relaxing the hollow face, and Figure 10iii corresponds to the achiral bridge face described in Figure 8b. Comparing the orientation of the symmetry planes of CH_3 in these arrangements, it is observed that they differ in rotations around the adsorption site and the S−C axis. This asymmetry is reflected in the angle made by the sulfur−carbon bond and each one of the Ag atoms involved in the bridge, Ag(1)−S−C and Ag(2)−S−C. The calculated angles are in Table 2, as well as the γ angle defined previously here as the smallest angle between one of the symmetry planes of CH_3 and one of Ag_{55}. From Table 2 we observe that as γ becomes larger the difference between the two angles Ag(1)−S−C and Ag(2)−S−C also does. The values of $\gamma \neq 0$ means that the symmetry of the whole compound is broken, giving rise to optical activity. Therefore, it is interesting to compare CD spectra of similar relaxed isomers, but having different γ or asymmetry.

Figure 11 shows CD spectra for the three bridge−face isomers described above, where the main difference

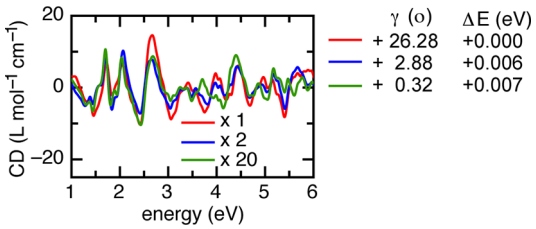

Figure 11. CD spectra of lower-energy bridge−face isomers described in Figure 10 and different γ values. Blue and green spectra have been rescaled by a factor of 2 and 20, respectively.

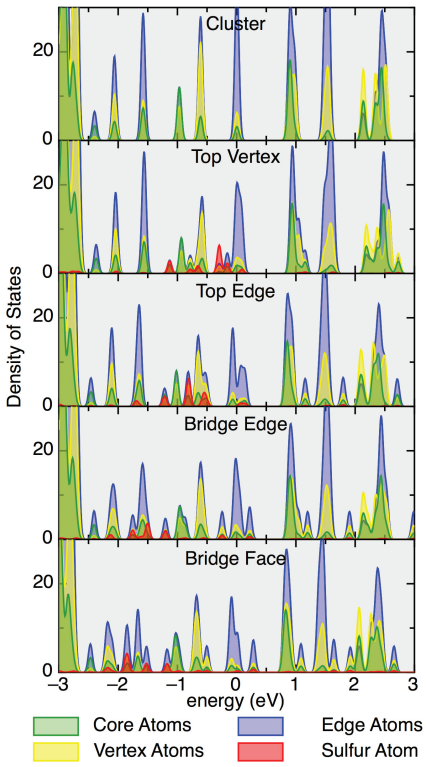

Figure 12. Contributions to the DOS from core atoms (excluding the central atom), outside edge atoms, outside vertex atoms, and the sulfur atom for bare and top and bridges low-energy isomers. The Fermi level is set at 0 eV.

among them is the value of γ, as shown in Table 2. We have found that the order of magnitude of the CD spectrum is directly related with the value of γ. Indeed, CD spectra of bridge face cases ii and iii have been rescaled by a factor of 2 and 20, respectively. It is noteworthy that all CD spectra have similar line-shapes, even the case for an almost null γ. This shows that CD line-shape is defined by the adsorption site, while the intensity is modulated with the asymmetry or γ value of a given configuration.

To understand the origin on the differences in CD line-shapes and intensities, we take a look at the electronic dependence by calculating the density of states (DOS) for each case discussed here. In Figure 12, we display DOS where the contribution from Ag atoms of different coordination number is shown separately. Therefore, contributions from core Ag atoms with coordination number (12) are shown in green, while contributions from outside edge atoms are in blue and outside vertex atoms are in yellow, with coordination numbers (8) and (6), respectively. The contribution from the sulfur atom is also shown in red. As we mentioned above, large symmetry in bare clusters leads to highly degenerated molecular-like states. Although contributions from the three different Ag silver atoms are found in all peaks, it is observed that Ag core atoms contribute more at low energies (occupied electronics states), while outer shell edge atoms play an important role at large energies (empty electronic states). Despite that molecular adsorption occurs on one or two atoms only, the binding of the sulfur distorts the whole electronic density, even the contribution belonging to core atoms. As we can appreciate from Figure 12, the degeneration of occupied and empty states breaks down upon adsorption, where the states extend over energies not allowed before. Also, we observe that sulfur states have an important contribution to DOS. For instance, in both top cases sulfur states are just below the Fermi level but localized mainly in an energy range from −1.5 to 0 eV, where the distortion of Ag states are more evident. Notice that these occupied states are involved in the appearance of CD in Figure 6, where peaks around 2 eV are more intense. Now, in both bridge cases sulfur states and the distorted Ag ones are now less localized, extending in a wider range of energies. This fact can explain in part that bridge CD spectra extend over the whole range of energies and show an almost constant intensity, as discussed in Figure 9. However, to get CD not only electric dipolar transitions are necessary, but also magnetic ones as shown in eq 3, where the intensity would be given based on how parallel these resulting dipoles are.

CONCLUSIONS

The optical activity of a single SCH_3 molecule adsorbed on Ag_{55} with icosahedral geometry is studied for different adsorption sites and molecule orientations. Although the NP and molecule are achiral, the lowest-energy configuration $Ag_{55}SCH_3$ is reached in such way that neither symmetry plane of Ag_{55} coincides with any symmetry plane of SCH_3, resulting chiral and thus optically active. We have discussed how chiral assemblies can emerge from achiral constituents, where the atomic coordination number plays an important role. Circular dichroism (CD) was found in the UV−visible region for chiral configurations. It is concluded that CD spectra strongly depends on the final morphology of the complex, where the adsorption site determines the line-shape and magnitude, while the molecule orientation tunes the maxima and minima intensity. For instance, CD maximum is found when for a given adsorption site, the molecule reaches the largest

asymmetric stable configuration. It is concluded that optical activity depends not only on the intrinsic chirality associated to the molecule or nanoparticle, but also on the symmetry breaking given by the adsorption site and orientation of the molecule. Since geometry has a strong influence on optical activity on these compounds, it is expected to find a quite similar behavior for gold nanocluster to those of silver discussed here.

METHODOLOGY AND COMPUTATIONAL DETAILS

Molecular Dynamics Simulations. Using density functional theory (DFT) within the general-gradient approximation (GGA) and Perdew–Burke–Ernzerhof (PBE) exchange-correlation functional, scalar-relativistic norm-conserving pseudopotentials and a double-ζ polarized basis set of numerical atomic orbitals, we perform molecular dynamics simulations for the configurations described above, exploring many different molecule orientations. By considering unconstrained relaxations with atomic forces of 0.01 eV/Å or less, optimized lowest-energy configurations are obtained. DFT calculations were performed using the siesta code,[46] which has been successfully proved for silver NPs,[47] and ligand-protected gold nanoclusters.[29]

Circular Dichroism (CD) Calculations. Once the low-energy isomers are obtained for each configuration, CD spectra are calculated as follow. CD is an optical property that only chiral objects exhibit, and *ab initio* computations are necessary for its reliable interpretation. Here, we employ a time-perturbed first-principles method recently developed to study the natural optical activity of nanostructures, making large-scale calculations feasible.[48] This methodology provides theoretical support for the quantification, understanding, and prediction of chirality and its measurement in complex nanostructures composed with a large number of atoms.[12,17] Experimentally, CD can be measured as the difference between left and right molar extinctions, $\Delta\varepsilon = \varepsilon_L - \varepsilon_R$. Theoretically, CD is given by a third order nonlocal electromagnetic term:[11]

$$\Delta\varepsilon(\omega) = \frac{0.1343 \times 10^{-5}}{3300}\beta(\omega)\tilde{\nu}^2 \quad (1)$$

where $\tilde{\nu}$ (cm^{-1}) is the wavenumber, and

$$\beta(\omega) = -\frac{1}{3\omega}\mathrm{Tr}[\mathrm{Re}(\tilde{G}_{\alpha\beta}(\omega))] \quad (2)$$

which has units of a_0^4, where a_0 is the Bohr radius (in atomic units), Re means the real part, and Tr is the trace. The above expression was obtained from a time-dependent perturbation theory, where the Hamiltonian was expressed through an electromagnetic multipolar expansion of vector and scalar potentials. Therefore, CD spectrum is computed once the Rosenfeld equation of the rotational strength is calculated:[11]

$$\tilde{G}_{\alpha\beta} \sim \sum_{j\neq n}\left\{\frac{\langle n|\mu_\alpha|j\rangle\langle j|m_\beta|n\rangle}{\omega_{jn}-\omega} + \frac{\langle n|m_\alpha|j\rangle\langle j|\mu_\beta|n\rangle}{\omega_{jn}+\omega}\right\} \quad (3)$$

where the matrix elements $\langle n|\mu_\alpha|j\rangle$ and $\langle j|m_\beta|n\rangle$ of the respective components, α and β, of the electric (μ) and magnetic (m) dipole moments, correspond to transitions from ground states $|n\rangle$ with energy ε_n, to excited states $|j\rangle$ with energy ε_j; here, ω is the frequency of the incident radiation field and $\hbar\omega_{jn} = \varepsilon_j - \varepsilon_n$. Although chirality may, in principle, be deduced from the CD spectrum, the task of computing the rotational strengths for various transitions is by no means easy. For more details see ref 48. This methodology has been proved for fullerenes,[12] carbon nanotubes,[17] and ligand-protected gold NPs,[20,28,29,34] showing excellent agreement with experiments and other time-dependent DFT calculations.

Conflict of Interest: The authors declare no competing financial interest.

Acknowledgment. This work has been supported by DGAPA-UNAM PAPIIT IN104212 and CONACyT 179454 grants.

REFERENCES AND NOTES

1. Huang, X.; El-Sayed, I. H.; Qian, W.; El-Sayed, M. A. Cancer Cell Imaging and Photothermal Therapy in the Near-Infrared Region by Using Gold Nanorods. *J. Am. Chem. Soc.* **2006**, *128*, 2115–2120.
2. Zhang, J.; Noguez, C. Plasmonic Optical Properties and Applications of Metal Nanostructures. *Plasmonics* **2008**, *3*, 127–150.
3. Haruta, M.; Daté, M. Advances in the Catalysis of Au Nanoparticles. *Appl. Catal., A* **2001**, *222*, 427–437.
4. Daniel, M.-C.; Astruc, D. Gold Nanoparticles: Assembly, Supramolecular Chemistry, Quantum-Size-Related Properties, and Applications Toward Biology, Catalysis, and Nanotechnology. *Chem. Rev.* **2004**, *104*, 293–346.
5. Jain, P. K.; Lee, K. S.; El-Sayed, I. H.; El-Sayed, M. A. Calculated Absorption and Scattering Properties of Gold Nanoparticles of Different Size, Shape, and Composition: Applications in Biological Imaging and Biomedicine. *J. Phys. Chem. B* **2006**, *110*, 7238–7248.
6. Clarke, M. L.; Chou, S. G.; Hwang, J. Monitoring Photothermally Excited Nanoparticles *via* Multimodal Microscopy. *J. Phys. Chem. Lett.* **2010**, *1*, 1743–1748.
7. Zhang, J. Z. Biomedical Applications of Shape-Controlled Plasmonic Nanostructures: A Case Study of Hollow Gold Nanospheres for Photothermal Ablation Therapy of Cancer. *J. Phys. Chem. Lett.* **2010**, *1*, 686–695.
8. Zhang, J.; Albelda, M. T.; Liu, Y.; Canary, J. W. Chiral Nanotechnology. *Chirality* **2005**, *17*, 404–420.
9. López-Lozano, X.; Pérez, L. A.; Garzón, I. L. Enantiospecific Adsorption of Chiral Molecules on Chiral Gold Clusters. *Phys. Rev. Lett.* **2006**, *97*, 233401.
10. Modi, S.; Bhatia, D.; Simmel, F. C.; Krishnan, Y. Structural DNA Nanotechnology: From Bases to Bricks, From Structure to Function. *J. Phys. Chem. Lett.* **2010**, *1*, 1994–2005.
11. Barron, L. D. *Molecular Light Scattering and Optical Activity*, 2nd ed.; Cambridge University Press: Cambridge, UK, 2004.
12. Hidalgo, F.; Noguez, C. Optically Active Nanoparticles: Fullerenes, Carbon Nanotubes, and Metal Nanoparticles. *Phys. Status Solidi B* **2010**, *247*, 1889–1897.
13. Yao, H. Optically Active Gold Nanoclusters. *Curr. Nanosci.* **2008**, *4*, 92–97.
14. Noguez, C.; Garzón, I. L. Optically Active Metal Nanoparticles. *Chem. Soc. Rev.* **2009**, *38*, 757–771.
15. Gautier, C.; Bürgi, T. Chiral Gold Nanoparticles. *Chem. Phys. Chem.* **2009**, *10*, 483–492.
16. Sánchez-Castillo, A.; Román-Velázquez, C. E.; Noguez, C. Optical Circular Dichroism of Single-Wall Carbon Nanotubes. *Phys. Rev. B* **2006**, *73*, 045401.
17. Sánchez-Castillo, A.; Noguez, C. Understanding Optical Activity in Single-Walled Carbon Nanotubes from First-Principles Studies. *J. Phys. Chem. C* **2010**, *114*, 9640–9644.
18. Kumar, S.; Bolan, M. D.; Bigioni, T. P. Glutathione-Stabilized Magic-Number Silver Cluster Compounds. *J. Am. Chem. Soc.* **2010**, *132*, 13141–13143.
19. Jin, R.; Qian, H.; Wu, Z.; Zhu, Y.; Zhu, M.; Mohanty, A.; Garg, N. Size Focusing: A Methodology for Synthesizing Atomically Precise Gold Nanoclusters. *J. Phys. Chem. Lett.* **2010**, *1*, 2903–2910.
20. Noguez, C.; Sánchez-Castillo, A.; Hidalgo, F. Role of Morphology in the Enhanced Optical Activity of Ligand-Protected Metal Nanoparticles. *J. Phys. Chem. Lett.* **2011**, *2*, 1038–1044.
21. Schaaff, T. G.; Whetten, R. L. Giant Gold Glutathione Cluster Compounds: Intense Optical Activity in Metal-Based Transitions. *J. Phys. Chem. B* **2000**, *104*, 2630–2641.

22. Andreiadis, E. S.; Vitale, M. R.; Mezailles, N.; Le Goff, X.; Le Floch, P.; Toullec, P. Y.; Michelet, V. Chiral Undecagold Clusters: Synthesis, Characterization and Investigation in Catalysis. *Dalton Trans.* **2010**, *39*, 10608–10616.
23. Molotsky, T.; Tamarin, T.; Ben Moshe, A.; Markovich, G.; Kotlyar, A. B. Synthesis of Chiral Silver Clusters on a DNA Template. *J. Phys. Chem. C* **2010**, *114*, 15951–15954.
24. Shukla, N.; Bartel, M. A.; Gellman, A. J. Enantioselective Separation on Chiral Au Nanoparticles. *J. Am. Chem. Soc.* **2010**, *132*, 8575–8580.
25. Yao, H.; Nishida, N.; Kimura, K. Conformational Study of Chiral penicillamine Ligand on Optically Active Silver Nanoclusters with IR and VCD Spectroscopy. *Chem. Phys.* **2010**, *368*, 28–37.
26. Mori, K.; Kondo, Y.; Yamashita, H. Synthesis and Characterization of FePd Magnetic Nanoparticles Modified with Chiral BINAP Ligand as a Recoverable Catalyst Vehicle for the Asymmetric Coupling Reaction. *Phys. Chem. Chem. Phys.* **2009**, *11*, 8949–8954.
27. Garzón, I. L.; Reyes-Nava, J. A.; Rodríguez-Hernández, J. I.; Sigal, I.; Beltrán, M. R.; Michaelian, K. Chirality in Bare and Passivated Gold Nanoclusters. *Phys. Rev. B* **2002**, *66*, 073403.
28. Santizo, I. E.; Hidalgo, F.; Pérez, L. A.; Noguez, C.; Garzón, I. L. Intrinsic Chirality in Bare Gold Nanoclusters: The Au_{34} Case. *J. Phys. Chem. C* **2008**, *112*, 17533–17539.
29. Hidalgo, F.; Sánchez-Castillo, A.; Garzón, I. L.; Noguez, C. First-Principles Calculations of Circular Dichroism of Ligand-Protected Gold Nanoparticles. *Eur. Phys. J. D* **2009**, *52*, 179–182.
30. Román-Velázquez, C. E.; Noguez, C.; Garzón, I. L. Circular Dichroism Simulated Spectra of Chiral Gold Nanoclusters: A Dipole Approximation. *J. Phys. Chem. B* **2003**, *107*, 12035–12038.
31. Heaven, M. W.; Dass, A.; White, P. S.; Holt, K. M.; Murray, R. W. Crystal Structure of the Gold Nanoparticle $[N(C_8H_{17})_4][Au_{25}(SCH_2CH_2Ph)_{18}]$. *J. Am. Chem. Soc.* **2008**, *130*, 3754–3755.
32. Zhu, M.; Aikens, C. M.; Hollander, F. J.; Schatz, G. C.; Jin, R. Correlating the Crystal Structure of a Thiol-Protected Au_{25} Cluster and Optical Properties. *J. Am. Chem. Soc.* **2008**, *130*, 5883–5885.
33. Tsukuda, T.; Tsunoyama, H.; Negishi, Y.; In *Metal Nanoclusters in Catalysis and Materials Science: The Issue of Size Control*; Elsevier: Amsterdam, 2008; pp 373−382.
34. Sánchez-Castillo, A.; Noguez, C.; Garzón, I. L. On the Origin of the Optical Activity Displayed by Chiral-Ligand-Protected Metallic Nanoclusters. *J. Am. Chem. Soc.* **2010**, *132*, 1504–1505.
35. Goldsmith, M.-R.; George, C. B.; Zuber, G.; Naaman, R.; Waldeck, D. H.; Wipf, P.; Beratan, D. N. The Chiroptical Signature of Achiral Metal Clusters Induced by Dissymmetric Adsorbates. *Phys. Chem. Chem. Phys.* **2006**, *8*, 63–67.
36. Dolamic, I.; Knoppe, S.; Dass, A.; Bürgi, T. First Enantioseparation and Circular Dichroism Spectra of Au_{38} Clusters Protected by Achiral Ligands. *Nat. Commun.* **2012**, *3*, 798.
37. Lopez-Acevedo, O.; Tsunoyama, H.; Tsukuda, T.; H., H.; Aikens, C. M. Chirality and Electronic Structure of the Thiolate-Protected Au38 Nanocluster. *J. Am. Chem. Soc.* **2010**, *132*, 8210–8218PMID: 20499877.
38. Govorov, A. O.; Fan, Z.; Hernandez, P.; Slocik, J. M.; Naik, R. R. Theory of Circular Dichroism of Nanomaterials Comprising Chiral Molecules and Nanocrystals: Plasmon Enhancement, Dipole Interactions, and Dielectric Effects. *Nano Lett.* **2010**, *10*, 1374–1382.
39. Li, T.; Park, H. G.; Lee, H.-S.; Choi, S.-H. Circular Dichroism Study of Chiral Biomolecules Conjugated with Silver Nanoparticles. *Nanotechnology* **2004**, *15*, S660.
40. Nan, J.; Yan, X.-P. A Circular Dichroism Probe for L-Cysteine Based on the Self-Assembly of Chiral Complex Nanoparticles. *Chem.—Eur. J.* **2010**, *16*, 423–427.
41. Lieberman, I.; Shemer, G.; Fried, T.; Kosower, E.; Markovich, G. Plasmon-Resonance-Enhanced Absorption and Circular Dichroism. *Angew. Chem., Int. Ed.* **2008**, *47*, 4855–4857.
42. Zhao, L.; Jensen, L.; Schatz, G. C. Pyridine−Ag_{20} Cluster: A Model System for Studying Surface-Enhanced Raman Scattering. *J. Am. Chem. Soc.* **2006**, *128*, 2911–2919.
43. Cotton, F. A. *Chemical Applications of Group Theory*, 3rd ed.; John Wiley and Sons: New York, 1990.
44. Harb, M.; Rabilloud, F.; Simon, D. Optical Response of Silver Nanoclusters Complexed with Aromatic Thiol Molecules: A Time-Dependent Density Functional Study. *J. Phys. B* **2011**, *44*, 035101.
45. The CD expression results from the inspection of the parity inversion of the extinction coefficient that contains all multipolar contributions from the time-perturbed Hamiltonian. This parity inversion operation results from considering electric fields circularly polarized to the right and then to the left. In this expansion, in decreasing order of magnitude, the first term is related to the optical absorption and scattering given by the square magnitude of the electric-dipole, the second term is related with the Faraday rotation given by the product of the electric-dipole and electric-quadrupole. The third term is related to optical activity and is given by the product of the electric-dipole and magnetic-dipole named rotational strength; and so on. In the absence of magnetic fields, the first two terms are symmetric under parity inversion, such that they do not contribute to CD, which is defined as the differences in extinction between left and right circularly polarized light. On the other hand, the third term being 2 orders of magnitude smaller than absorption is practically undetectable by measuring extinction. This is the main reason that is not possible to distinguish from different molecule orientations by just looking at optical absorption even when CD is not null. For a complete explanation please refer to ref 11.
46. Soler, J. M.; Artacho, E.; Gale, J. D.; García, A.; Junquera, J.; Ordejón, P.; Sánchez-Portal, D. The SIESTA Method for *ab Initio* Order-N Materials Simulation. *J. Phys.: Condens. Matter* **2002**, *14*, 2745.
47. Angulo, A. M.; Noguez, C. Atomic Structure of Small and Intermediate-Size Silver Nanoclusters. *J. Phys. Chem. A* **2008**, *112*, 5834–5838.
48. Hidalgo, F.; Sánchez-Castillo, A.; Noguez, C. Efficient First-Principles Method for Calculating the Circular Dichroism of Nanostructures. *Phys. Rev. B* **2009**, *79*, 075438.